Conjugates of Superoxide Dismutase 1 with Amphiphilic Poly(2-oxazoline) Block Copolymers for Enhanced Brain Delivery: Synthesis, Characterization and Evaluation in Vitro and in Vivo

Jing Tong,[†,‡,§] Xiang Yi,[§,‖] Robert Luxenhofer,[⊥] William A. Banks,[#] Rainer Jordan,[○] Matthew C. Zimmerman,[†,□] and Alexander V. Kabanov*,[‖,¶]

[†]Center for Drug Delivery and Nanomedicine, [‡]Department of Pharmaceutical Sciences, and [□]Department of Cellular and Integrative Physiology, University of Nebraska Medical Center (UNMC), Omaha, Nebraska 68198, United States
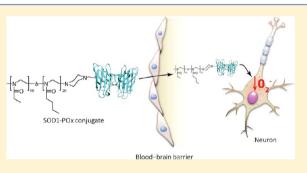
[‖]UNC Eshelman School of Pharmacy, University of North Carolina at Chapel Hill, Chapel Hill, North Carolina 27599, United States

[⊥]Functional Polymer Materials, Chemical Technology of Advanced Materials, Universität Würzburg, 97070 Würzburg, Germany

[#]GRECC—Veterans Affairs Puget Sound Health Care System, and Division of Gerontology & Geriatric Medicine, Department of Medicine, University of Washington, Seattle, Washington 98104, United States

[○]Professur für Makromolekulare Chemie, Department Chemie, Technische Universität Dresden, 01062 Dresden, Germany

[¶]Faculty of Chemistry, M.V. Lomonosov Moscow State University, 119899 Moscow, Russia

Ⓢ *Supporting Information*

ABSTRACT: Superoxide dismutase 1 (SOD1) efficiently catalyzes dismutation of superoxide, but its poor delivery to the target sites in the body, such as brain, hinders its use as a therapeutic agent for superoxide-associated disorders. Here to enhance the delivery of SOD1 across the blood−brain barrier (BBB) and in neurons the enzyme was conjugated with poly(2-oxazoline) (POx) block copolymers, P(MeOx-*b*-BuOx) or P(EtOx-*b*-BuOx), composed of (1) hydrophilic 2-methyl-2-oxazoline (MeOx) or 2-ethyl-2-oxazoline (EtOx) and (2) hydrophobic 2-butyl-2-oxazoline (BuOx) repeating units. The conjugates contained from 2 to 3 POx chains joining the protein amino groups via cleavable -(ss)- or noncleavable -(cc)-

linkers at the BuOx block terminus. They retained 30% to 50% of initial SOD1 activity, were conformationally and thermally stable, and assembled in 8 or 20 nm aggregates in aqueous solution. They had little if any toxicity to CATH.a neurons and displayed enhanced uptake in these neurons as compared to native or PEGylated SOD1. Of the two conjugates, SOD1-(cc)-P(MeOx-*b*-BuOx) and SOD1-(cc)-P(EtOx-*b*-BuOx), compared, the latter was entering cells 4 to 7 times faster and at 6 h colocalized predominantly with endoplasmic reticulum (41 ± 3%) and mitochondria (21 ± 2%). Colocalization with endocytosis markers and pathway inhibition assays suggested that it was internalized through lipid raft/caveolae, also employed by the P(EtOx-*b*-BuOx) copolymer. The SOD activity in cell lysates and ability to attenuate angiotensin II (Ang II)-induced superoxide in live cells were increased for this conjugate compared to SOD1 and PEG-SOD1. Studies in mice showed that SOD1−POx had ca. 1.75 times longer half-life in blood than native SOD1 (28.4 vs 15.9 min) and after iv administration penetrated the BBB significantly faster than albumin to accumulate in brain parenchyma. The conjugate maintained high stability both in serum and in brain (77% vs 84% at 1 h postinjection). Its amount taken up by the brain reached a maximum value of 0.08% ID/g (percent of the injected dose taken up per gram of brain) 4 h postinjection. The entry of SOD1-(cc)-P(EtOx-*b*-BuOx) to the brain was mediated by a nonsaturable mechanism. Altogether, SOD1−POx conjugates are promising candidates as macromolecular antioxidant therapies for superoxide-associated diseases such as Ang II-induced neurocardiovascular diseases.

KEYWORDS: *superoxide dismutase 1, polyoxazoline, reactive oxygen species, oxidative stress, neurons, blood−brain barrier, polymer therapeutics, endocytosis, pharmacokinetics*

1. INTRODUCTION

Elevation of reactive oxygen species (ROS) levels in the central nervous system (CNS) is related to multiple severe human diseases such as stroke, neurodegenerative disorders and neurocardiovascular diseases.[1−3] Specifically superoxide ($O_2^{•−}$) can cause oxidative damage to cellular components, induce apoptosis and tissue injury, and participate in redox

signaling pathways leading to detrimental physiological effects. For example, the endogenous vasoconstrictor peptide angio-

tensin II (Ang II) induces an increase in intracellular superoxide in distinct regions of the brain, leading to increased neuronal activation and sympathoexcitation, which play a key role in the pathogenesis of neurocardiovascular diseases such as hypertension and heart failure.[1−3] Catalytic or noncatalytic superoxide scavengers can remove the excess intracellular superoxide, attenuate oxidative injury and inhibit redox signaling, and thus serve as potential therapeutic antioxidants for multiple superoxide-related diseases including Ang II-dependent neurocardiovascular diseases.[3−7]

The enzyme superoxide dismutase 1 (SOD1, also known as Cu,Zn/SOD) efficiently catalyzes the dismutation of superoxide into oxygen and hydrogen peroxide. It is a stable homodimer of identical 16 kDa subunits held together primarily by hydrophobic interactions and cofactored with copper and zinc.[8,9] SOD1 has high conformational and thermal stability and, thus, has great potential to be developed as a therapeutic agent for superoxide-related diseases.[10] However, like many other therapeutic proteins, SOD1 has a very short blood circulation time and is incapable of crossing the blood–brain barrier (BBB) or neuronal cell membranes to reach its target sites.[11] Conjugation of SOD1 with poly(ethylene glycol) (PEGylation) significantly increased its retention time in plasma but did not significantly enhance its cellular delivery and transport across the BBB.[12−14] Alternatively, other conjugation strategies have been developed recently to enhance the cellular or brain delivery of SOD1, such as conjugation with targeting antibody to endothelial determinants,[15−18] cell penetrating peptide,[19] or BBB penetrating nanoparticles.[20]

One promising strategy to address this problem is to conjugate SOD1 with amphiphilic triblock copolymers such as poly(ethylene glycol)-b-poly(propylene glycol)-b-poly(ethylene glycol) (PEG-PPG-PEG), known as Pluronic or poloxamer. It has been shown that conjugation with Pluronics can increase the cellular delivery and BBB permeability of multiple proteins while also increasing their in vivo stability and blood circulation time.[9,21−24] We found that SOD1−Pluronic conjugates exhibit significantly enhanced neuronal delivery as compared to native SOD1 or PEGylated SOD1 (SOD1−PEG).[9] The detailed in vivo therapeutic potential of protein−Pluronic conjugates is currently under investigation in several animal disease models.

Recently, amphiphilic poly(2-oxazoline) (POx) block copolymers were developed as an alternative to Pluronics for protein modification.[25] POx are synthesized by living cationic ring-opening polymerization (LCROP) of 2-oxazoline monomers. This highly living and versatile polymerization technique yields well-defined POx with low dispersity and can be used to produce a variety of structures bearing defined functional end and pendant groups.[25−28] The hydrophilic/hydrophobic balance of POx can be tuned over a broad range by varying the monomer unit side chains and architecture. This is expected to be critical to modulate cellular binding of the protein−POx conjugate while maintaining its stability.[25,29] Notably, POx display greater chemical stability compared to polyethers, such as PEG or Pluronic, which are prone to oxidative degradation.

In our previous study, a model protein, horseradish peroxidase (HRP), was conjugated with two block copolymers, one random copolymer and one homopolymer of POx. The block copolymer based HRP−POx conjugates exhibited significantly enhanced cellular binding and uptake compared to native HRP or homopolymer-based conjugates.[25] In the present study, we synthesized SOD1−POx conjugates using the same pair of POx block copolymers to evaluate the impact of

the conjugation on brain delivery of SOD1. Moreover, the amphiphilic POx were conjugated with SOD1 by means of biodegradable and nonbiodegradable linkers. The paper presents new data on (1) synthesis and characterization of SOD1−POx conjugates by multiple analytical and biophysical techniques; (2) the cytotoxicity, cellular uptake, and intracellular trafficking of SOD1−POx conjugates; (3) the intracellular activity of a selected SOD1−POx conjugate in CATH.a neuronal cells; and finally, (4) the pharmacokinetics, brain delivery, and tissue distribution of SOD1−POx conjugate in a mouse model.

2. MATERIALS AND METHODS

2.1. Materials. Poly(2-methyl-2-oxazoline)$_{50}$-*block*-poly(2-butyl-2-oxazoline)$_{20}$ [P(MeOx-*b*-BuOx)] and poly(2-ethyl-2-oxazoline)$_{50}$-*block*-poly(2-butyl-2-oxazoline)$_{20}$ [P(EtOx-*b*-BuOx)] were synthesized under inert conditions by a two-step living cationic polymerization as described before.[25] SOD1 and SOD1−PEG from bovine erythrocytes, *N,N*-dimethylformamide (DMF), anhydrous dichloromethane, ethanol, sinapic acid, acetonitrile, trifluoroacetic acid (TFA), pyrogallol, 2,4,6-trinitrobenzenesulfonic acid (TNBS), N-6,2′-O-dibutyryl adenosine 3′,5′-cyclic-monophosphate (AMP), sucrose, methyl-beta-cyclodextrin (MBCD), superoxide anion assay kit, Ang II, chloramine-T, and trichloroacetic acid were purchased from Sigma-Aldrich Co. (St. Louis, MO). Dithiobis(succinimidyl propionate) (DSP) and disuccinimidyl propionate (DSS) were from Pierce Biotech Co. (Rockford, IL). Sephadex LH-20 gel and Illustra NAP-5 columns were from GE Healthcare (Waukesha, WI). Amicon ultra-4 centrifugal filter units, MWCO 10K, 13 mm syringe filter (0.22 and 0.45 μm), micro BCA protein assay kit, bovine serum albumin (BSA), 3,3′,5,5′-tetramethylbenzidine (TMB), TMB stop solution, NUNC immuno 96-well plate, NUNC LumiNunc 96-well plate, and NUNC Lab-Tek II chambered slide were from Thermo Fisher Scientific (Waltham, MA). Tris-HCL Precast gels (12%), Biosafe coomassie stain and SYPRO Ruby stain solution were from Bio-Rad (Hercules, CA). Primary bovine SOD1 antibody (rabbit IgG) and secondary HRP-conjugated antibody to rabbit IgG were from Abcam (Cambridge, MA). Alexa Fluor 647 protein labeling kit, Hoechst 33342, MitoTracker, LysoTracker, ER-Tracker, Alexa Fluor 488-conjugated transferrin (Tf), and cholera toxin B (CTB) were from Invitrogen (Carlsbad, CA). Methoxycarbonyl-2,2,5,5-tetramethylpyrrolidine (CMH), deferoxamine methanesulfonate salt (DF), and diethyldithiocarbamic acid sodium (DETC) were from Noxygen Science Transfer & Diagnostics GmbH (Elzach, Germany).

2.2. Devices. Size-exclusion chromatography (SEC) was performed on an ÄKTA fast protein liquid chromatography (ÄKTA FPLC) system with a Superdex 75 column (10 × 300 mm) from GE Healthcare and a Shimadzu high performance liquid chromatography (HPLC) system with a TSKgel G2000SWxl column (7.8 × 300 mm) from Tosoh Co. (Japan). Matrix-assisted laser desorption/ionization time-of-flight mass spectrometry (MALDI-TOF MS) was carried out with a MALDI-TOF-TOF 4800 system (Applied Biosystems, Foster City, CA) in positive reflector mode. An Aviv circular dichroism (CD) model 202SF spectrometer (Aviv Biomedical, Inc., Lakewood, NJ) was used for the characterization of secondary structures of SOD1 and SOD1−POx conjugates. A Microcal VP-DSC differential scanning calorimeter (Microcal, Northampton, MA) was used for the measurement of protein

melting curves. Particle size and size distribution of protein solutions were determined by dynamic light scattering (DLS) using a Nano series Zetasizer (Malvern Instrument Inc., Westborough, MA). Confocal microscopy was carried out with a LSM 710 confocal imaging system (Carl Zeiss, Peabody, MA). Flow cytometry was carried out with a LSR II flow cytometer (BD Biosciences, San Jose, CA). Electron paramagnetic resonance (EPR) spectroscopy was performed with a Bruker Biospin e-scan spectrometer (Bruker, Billerica, MA).

2.3. Synthesis and Purification of SOD1−POx. SOD1−POx conjugates were synthesized analogously to the procedure described previously.[25] Briefly, secondary amine of the piperazine-terminated POx was reacted with homofunctional linkers DSS or DSP. 55 mg of POx was reacted with a 20-fold molar excess of DSS in DMF. The mixture was supplemented with sodium borate buffer (0.1 M, pH 8.0) and reacted for 30 min at rt. The activated POx was purified by gel filtration on a Sephadex LH-20 column in dry dichloromethane, and 15 mg of SOD1 in sodium borate buffer (0.1 M, pH 8.0) was added. The reaction mixture was incubated overnight at 4 °C. The resulting SOD1−POx conjugates were purified by FPLC using 0.1 M phosphate buffered saline (PBS, pH 7.4) as the mobile phase and UV detection at 254 nm. The conjugates were desalted and lyophilized for further characterization.

2.4. Characterization of SOD1−POx Conjugates.
2.4.1. Chromatography. Purity and aggregation of SOD1−POx were analyzed by SEC. The conjugates were analyzed using a mobile phase consisting of methanol (5%) and pH 6.8, 0.1 M NaH_2PO_4, 0.2 M NaCl buffer (95%), and UV detection at 220 nm.

2.4.2. Mass Spectrometry. Molar mass of SOD1−POx was determined by matrix-assisted laser desorption/ionization time-of-flight mass spectroscopy (MALDI-TOF MS) using saturated sinapic acid solution in 50% acetonitrile and 0.1% aqueous TFA as the matrix. The mass spectrometer was calibrated against insulin (5729.61 Da) and albumin (66,429.09 Da).

2.4.3. Electrophoresis. Sodium dodecyl sulfate polyacrylamide gel electrophoresis (SDS−PAGE) analysis was performed as described before.[25] The gel was stained by Biosafe coomassie stain for 1 h and destained in water.

2.4.4. Degree of Modification by TNBS Assay. The degree of protein modification was determined by a TNBS assay as described before.[25] Briefly, 10 μL of SOD1 or SOD1−POx solutions (0.1−0.6 mg/mL) were mixed with 10 μL of TNBS solution (1.7 mM) in 80 μL of sodium borate buffer (0.1 M, pH 9.5) and incubated at 37 °C for 2 h. The absorbance at 405 nm was measured using a microplate reader (Spectra Max M5, MDS, CA). The degree of modification (average number of modified amino groups) was calculated according to

$$S = 22 \times \frac{(A_{native}/C_{native} - A_{modified}/C_{modified})}{A_{native}/C_{native}} \quad (1)$$

where A_{native} and $A_{modified}$ are the absorbencies and C_{native} and $C_{modified}$ are the concentrations of SOD1 and SOD1−POx respectively. The total number of primary amino groups including lysine residues and terminal amine group of a SOD1 dimer is 22.

2.4.5. Enzymatic Activity by Pyrogallol Auto-Oxidation Assay. Pyrogallol auto-oxidation assay was used to quantify the residual enzymatic activity of SOD1−POx as described before.[9] Briefly, 20 μL of 0.0002−200 μg/mL SOD1 or SOD1−POx was mixed with 20 μL of freshly prepared pyrogallol solution

(0.5 mg/mL) and supplemented with 180 μL of Tris-HCl buffer (0.1 M, pH 8) containing 1 mM diethylene triamine pentaacetic acid. Deionized water (DIH_2O) without enzyme and/or without pyrogallol was used as the control. The reaction mixtures were prepared in triplicate, and the rates of autoxidation were measured immediately by recording the increases of absorbance at 420 nm up to 10 min. The inhibition rate (%) was calculated by

$$I = [(S_1 - S_S)/(S_1 - S_2)] \times 100\% \quad (2)$$

where S_1 is the slope for enzyme-free water with pyrogallol, S_2 is the slope for enzyme-free water without pyrogallol, and S_S is the slope of the sample with pyrogallol. The half-maximum inhibitory concentration (IC_{50}) and the number of SOD activity unit per 1 mg of protein were calculated. The residual activity of SOD1−POx was expressed as the percentage of unit number of unmodified SOD1.

2.4.6. Circular Dichroism (CD). SOD1 or SOD1−POx was dissolved in PBS buffer (pH 7.4) at 0.5 mg/mL. CD spectra were recorded between 200 and 260 nm using an Aviv CD spectrometer with a cuvette of 0.1 cm path length. Spectra were recorded in 1 nm decrements, and the given spectra correspond to the average of three wavelength scans using the pure solvent as the background. The mean residue molar ellipticity $[\theta]$ was calculated by

$$[\theta] = (\theta M)/(Cl) \quad (3)$$

where θ is the observed ellipticity (deg), M, the mean residue molecular weight (g/mol), C, the protein concentration (g/mL), and l, the optical path length (cm).[25]

2.4.7. Differential Scanning Calorimetry (DSC). Melting curves of SOD1 or SOD1−POx solution were obtained on a Microcal DSC. SOD1 or SOD1−POx was dissolved in PBS buffer (pH 7.4) at 2.0 mg/mL. Melting curves were obtained from 10 to 110 °C in 0.2 °C increments. Transition temperatures (T_m) of SOD1 and SOD1−POx at which 50% of the protein denatured were obtained.[30]

2.4.8. Dynamic Light Scattering (DLS). Aggregation of SOD1 or SOD1−POx was analyzed by photon correlation spectroscopy (i.e., DLS) in a thermostatic cell at a scattering angle of 90°. SOD1 or SOD1−POx was dissolved in PBS buffer (pH 7.4) at 0.5 mg/mL. All measurements were performed at 25 °C. Intensity-based and volume-based size distributions were generated by the software provided by the manufacturer.

2.5. Cell Culture. CATH.a neuronal cells (ATCC CRL-11179) were seeded in 6-well plates at 500,000 cells/well or in 24-well plates at 150,000 cells/well (for cytotoxicity study) or in 2-well chambered slides (for confocal microscopy) in RPMI-1640 medium (Invitrogen, Carlsbad, CA) supplemented with 1% penicillin/streptomycin, 4% fetal bovine serum (Invitrogen, Carlsbad, CA), and 8% horse serum (Gibco, Life Tech., Grand Island, NY). CATH.a neurons were differentiated using 1 mM fresh AMP every 2 days. The cells were typically cultured for 6−8 days for full expression of Ang II receptors.

2.6. Cytotoxicity Assay. Neuronal toxicity of SOD1 and SOD1−POx was determined using a cell counting kit (Dojindo Molecular Technologies, Inc., Gaithersburg, MD) as described before.[9] Briefly, cells were seeded in 24-well plates and cultured. Culture medium was renewed with medium containing 80 μg/mL of SOD1 or SOD1−POx, or 100 μg/mL of PEG5000-*b*-poly(L-lysine)$_{50}$ (PEG-*b*-PLL) (Alamanda Polymers, Inc. Huntsville, AL) as a positive control. After that the cells were incubated with SOD1 or SOD1−POx for different periods (1−

24 h). The medium was renewed, and the cells were allowed to grow for an additional 48 h. The medium was renewed only this time containing 10% CCK-8 solution (2-(2-methoxy-4-nitrophenyl)-3-(4-nitrophenyl)-5-(2,4-disulfophenyl)-2H-tetra-zolium monosodium salt). The absorbance at 450 nm was recorded in a plate reader after 1 h incubation. The cell viability was calculated by

$$\text{cell viability (\%)} = \frac{A_{\text{sample}} - A_{\text{blank}}}{A_{\text{control}} - A_{\text{blank}}} \times 100\% \tag{4}$$

Each treatment was repeated four times, and data are presented as means ± SEM.

2.7. Cellular Uptake in CATH.a Neuronal Cells. Cellular uptake of SOD1, SOD1–PEG, and SOD1–POx was quantitatively analyzed using SOD1 ELISA. Briefly, cells were seeded in 24-well plates and cultured until the medium was replaced with fresh serum-free medium containing 80 μg/mL of SOD1, SOD1–PEG, or SOD1–POx. The cells were incubated with SOD1, SOD1–PEG, or SOD1–POx for different time periods (1–24 h). Cells were rinsed twice with PBS, collected, and resuspended. The cell suspensions were sonicated to prepare cell-free extracts. SOD1 ELISA was performed according to a protocol described previously, with some modifications.[31,32] Briefly, cell-free extract containing approximately 50–100 μg of cellular proteins was loaded into a NUNC immuno 96-well plate and immobilized by incubation at 37 °C for 2 h. At rt, the coated wells were incubated with 1% BSA in PBS for 2 h to block the remaining protein-binding sites. Next, the wells were incubated with primary bovine SOD1 antibody (1:500 dilution) for 2 h and then secondary HRP-conjugated antibody (1:120,000 dilution) for 2 h. Finally, the wells were incubated with TMB solution and supplemented with an equal volume of TMB stop solution. The absorbance at 450 nm was recorded in a plate reader. Different concentrations of SOD1, SOD1–PEG, or SOD1–POx were used to construct the calibration curve for each group. SOD1 concentration was normalized to the cellular protein concentration determined by MicroBCA assay. Each treatment was repeated three times, and data are presented as means ± SEM.

2.8. Fluorescent Labeling, Confocal Microscopy, and Flow Cytometry. *2.8.1. Fluorescent Labeling.* SOD1 and SOD1–POx were labeled with fluorescent probe Alexa Fluor 647 according to a protocol provided by the manufacturer. Briefly, 1 mg of SOD1 or SOD1–POx was mixed with the amine-reactive dye in sodium bicarbonate buffer (0.1 M, pH 8.0). The reaction was allowed to complete at rt for 1 h. The labeled protein was purified by gel filtration and lyophilized. The absorbance at 650 nm of the conjugate was measured by a plate reader. The degree of labeling (S, moles of dye per mole of protein) was calculated by

$$S = \frac{A_{650}D}{239000M} \tag{5}$$

where D is the dilution factor of the conjugate solution, M is the protein concentration, and 239,000 is the approximate molar extinction coefficient of the dye at 650 nm. The S values of both SOD1–POx conjugates were found to be similar: 0.67 for SOD1-(cc)-P(MeOx-b-BuOx) and 0.64 for SOD1-(cc)-P(EtOx-b-BuOx), and lower than that of SOD1 ($S = 1.67$).

Free P(EtOx-b-BuOx) was also labeled with the same dye using a modified protocol. Briefly, 4 mg of P(EtOx-b-BuOx) was mixed with the dye in DMF. The reaction mixture was supplemented with sodium borate buffer (0.1 M, pH 8.0) and reacted at rt for 2 h. The labeled polymer was purified by gel filtration and lyophilized. The absorbance at 650 nm was measured in a plate reader. The labeling efficiency was estimated to be 20%.

2.8.2. Visualization of Cellular Uptake by Confocal Laser Scanning Microscopy (CLSM). The cellular uptake of fluorescently labeled SOD1 and SOD1–POx was observed by CLSM. Briefly, cells were seeded in a 4-well chambered slide and cultured as described above until the medium was replaced with fresh, serum-free medium containing 80 μg/mL of fluorescently labeled SOD1 or SOD1–POx. Cells were incubated with fluorescently labeled SOD1 or SOD1–POx for different time periods (1–24 h). The cells were rinsed twice with PBS, and fluorescent images were collected. About 10–15 images containing 100–200 cells were recorded for each group and each time point, and the fluorescent intensity was quantified using a public domain imaging processing software (Image J from NIH).

2.8.3. Intracellular Localization. The intracellular localization of SOD1–POx was studied by CLSM. Briefly, cells were cultured as described above and treated with 80 μg/mL of fluorescently labeled SOD1–POx for 6 h. Organelles, including nucleus, mitochondria, lysosome, and endoplasmic reticulum (ER), were stained with specific fluorescent dyes for 30 min before imaging. Then, cells were rinsed twice with PBS and fluorescent images were taken. About 10–15 images containing 100–200 cells were collected for each group, and the colocalization ratio of fluorescently labeled SOD1–POx with each fluorescent dye was calculated using Image J.

2.8.4. Endocytosis. The endocytosis pathway of SOD1–POx was studied by CLSM and flow cytometry as described elsewhere.[33,34]

1. *Colocalization with Specific Endocytosis Markers.* Tf and CTB were used as the markers of clathrin-mediated endocytosis and lipid raft/caveolae-mediated endocytosis, respectively. Briefly, cells were cultured as described above and cotreated with both 80 μg/mL of fluorescently labeled SOD1–POx and fluorescently labeled transferrin or CTB for 6 h. The colocalization ratio of SOD1–POx with these endocytosis markers was analyzed using Image J.

2. *Inhibition of Specific Endocytosis Pathway.* Sucrose and MBCD were used as the specific inhibitors for clathrin-mediated endocytosis and lipid raft/caveolae-mediated endocytosis, respectively. For CLSM analysis, cells were cultured as described above. Then the cells were pretreated with 0.4 M sucrose or 4 mM MBCD for 30 min and then cotreated with fluorescently labeled SOD1–POx for 6 h. The cellular uptake of SOD1–POx was observed by CLSM, quantitatively analyzed (Image J), and compared with noninhibited controls. For flow cytometry analysis, cells were cultured in a 24-well plate as described above. The cells were pretreated with 0.4 M sucrose or 4 mM MBCD for 30 min and then cotreated with fluorescently labeled SOD1–POx for 6 h. The cellular uptake of SOD1–POx was expressed as the normalized mean fluorescence of gated cells and compared with noninhibited controls.

The endocytosis pathway of free P(EtOx-b-BuOx) was also studied by CLSM and flow cytometry in a similar way as described above. Cells were treated with 50 μg/mL of

fluorescently labeled P(EtOx-*b*-BuOx) for 1 h. The colocalization with Tf and CTB and the inhibition effects of sucrose and MBCD were analyzed.

2.9. Intracellular SOD Activity Assay. Intracellular activity of SOD1−POx was quantitatively determined using a luminol-based superoxide anion assay kit. The oxidation of luminol by superoxide results in the formation of chemiluminescence light, which can be further amplified by a specific enhancer. Active SOD can scavenge superoxide and thus inhibit the chemiluminescence signal. After 6−8 days culture, CATH.a neuronal cells in 6-well plates were incubated with 80 μg/mL of SOD1, SOD1−PEG, or SOD1−POx in fresh, serum-free medium for 12 h. Cells were washed twice with PBS, collected, and resuspended. The cell suspensions were sonicated to prepare cell-free extracts. The superoxide anion assay was performed according to a protocol provided by the manufacturer. Briefly, hypoxanthine-xanthine oxidase (HX-XO) catalytic system was used to generate superoxide. Samples contained xanthine oxidase, xanthine, luminol, enhancer, and cell-free extract or control. The reaction mixture was loaded into a LumiNunc 96-well plate, and the chemiluminescence signal was recorded in a plate reader immediately. Each treatment was repeated three times, and data are presented as means ± SEM.

2.10. Intracellular Electron Paramagnetic Resonance (EPR) Spectroscopy. The intracellular superoxide levels in CATH.a neuronal cells were quantitatively measured by EPR spectroscopy as described before, with some modifications.[35] After 6−8 days culture, CATH.a neuronal cells in 6-well plates were incubated with 80 μg/mL of SOD1, SOD1−PEG, or SOD1−POx in fresh, serum-free medium for 12 h. Cells were washed twice with EPR buffer (pH 7.4) and incubated with 1 mL of EPR buffer containing 200 μM CMH, a cell-permeable superoxide-sensitive spin probe for 1 h at 37 °C. After incubation, the cells were stimulated with 100 nM Ang II for 30 min. After stimulation ca. 0.9 mL of buffer was aspirated from the well, the cells were collected and resuspended with the remaining buffer, and cell suspensions were loaded into the EPR spectrometer to record the generation of superoxide for 10 min. To compensate for the difference in cell number between samples, the EPR amplitude of each sample was normalized to cell number determined by cell counting. Each treatment was repeated three times, and data are presented as means ± SEM.

2.11. Animal Studies. Animal study was carried out and data were analyzed by X.Y. as a visiting scholar at the University of Washington (in W.A.B.'s lab).

2.11.1. Radioactive Labeling (^{125}I-SOD1−POx). SOD1 or SOD1−POx samples were radioactively labeled by the chloramine-T method as previously described.[36] Briefly, SOD1 or SOD1−POx conjugate was incubated with 0.5 mCi Na^{125}I (Perkin-Elmer Life Sciences, Boston, MA) and 10 μg of chloramine-T freshly made for 60 s. The mixture was purified by Illustra NAP-5 columns. Fractions were collected in Eppendorf tubes that were precoated with 50 μL of 1% BSA in lactated Ringer's solution (LR-BSA) to prevent nonspecific absorbance. The radioactivities of fractions were counted in a PerkinElmer γ-counter and trichloroacetic acid (TCA) precipitation was conducted to determine the iodine association of labeled samples. Fractions containing more than 100,000 cpm/μL and in which the iodine association by TCA precipitation was more than 90% were used for the animal study. Similarly, BSA was labeled with Na^{131}I (Perkin-Elmer Life Sciences, Boston, MA) by the chloramine-T method.

Furthermore, electrophoresis was performed to confirm the iodination. Non-radioactively labeled samples or radioactively labeled samples containing 50,000 cpm were subjected to electrophoresis under nonreducing denaturing conditions. After fixing, the gel of non-radioactively labeled samples was stained in SYPRO Ruby solution; whereas the gel of radioactively labeled samples was dried and exposed to Blue Basic Autorad Film (Bioexpress, Kaysville, UT) overnight.

2.11.2. Animal Procedures. Pharmacokinetics (PK) and biodistribution studies were conducted with CD-1 male mice (8 to 10 weeks of age, Charles River Laboratories, Inc., Wilmington, MA). All experiments were conducted after institutional approval of the animal use subcommittee of the Veterans Affairs Puget Sound Health Care System, which subscribes to the National Institutes of Health Guide for Care and Use of Laboratory Animals. Mice were anesthetized by ip injection of urethane (40%). Radiolabeled sample was prepared and injected into the jugular vein. Blood from the carotid artery was collected at various time points. Mice were immediately decapitated and the whole brain and/or other tissues removed and weighed. The arterial blood was centrifuged, and the serum was collected. The radioactivity of tissue and serum samples was counted in a γ-counter. In some cases, a brain washout was performed before decapitating and the brain was collected. Briefly, after opening the abdomen, arterial blood was collected from the abdominal aorta. The thorax was then opened to expose the heart. The descending aorta was clamped, both jugular veins were severed, and LR-BSA was perfused over 1 min into the left ventricle of the heart. Finally, the mouse was decapitated and the whole brain removed and weighed for further experiments.

2.11.3. Serum Clearance and Influx Rate Across the Blood−Brain Barrier (BBB). Mice anesthetized with urethane received an iv injection of ^{125}I-SOD1 or ^{125}I-SOD1−POx with ^{131}I-albumin (300,000 cpm of each) into the jugular vein. Blood from the carotid artery and brain was collected at various time points between 2 and 240 min after injection. The radioactivities of brain and serum samples were counted in a γ-counter. The percent of the iv injected dose ID/μL in serum (% ID/μL) and the dose taken up per gram of brain at time t (% ID/g brain) were given by

$$\%ID/\mu L = \frac{C_p(t)}{ID} \times 100 \tag{6}$$

$$\%ID/g \text{ of brain} = \left(\frac{A_m}{C_p(t)} - V_{i(0)}\right)\frac{C_p(t)}{ID} \times 100 \tag{7}$$

where ID is the cpm iv injected. A_m and $C_p(t)$ are the cpm/g of brain and the cpm/μL of serum at time t, respectively.

The serum concentration (percent of the iv injected dose ID/μL in serum, % ID/μL) was plotted against time to describe the serum clearance. The slope between log(% ID/μL) and time was used to calculate the half time clearance from blood. Multiple-time regression analysis was applied to calculate the blood-to-brain unidirectional influx rate (K_i) of the radiolabeled compounds into the brain. The brain/serum ratios (μL/g) were plotted against exposure time estimated from

$$A_m/C_p(t) = K_i\left[\int_0^t C_p(t)\,dt\right]/C_p(t) + V_{i(0)} \tag{8}$$

where A_m and $C_p(t)$ are the cpm/g of brain and the cpm/μL of serum at time t, respectively. K_i was measured as the slope for
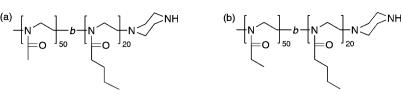
Figure 1. Structures of POx used in the present study: (a) P(MeOx-*b*-BuOx); (b) P(EtOx-*b*-BuOx).

the linear portion of the relation between brain/serum ratios and respective exposure times.[37,38] The exposure time was calculated as the area under the serum concentration time curve (integral part of eq 8) divided by serum concentration at time *t*. The *y*-intercept of the line represents $V_{i(0)}$, the distribution volume in the brain at *t* = 0.

2.11.4. Inhibition Study. To determine whether brain uptake of ^{125}I-SOD1−POx was saturable, an excess amount of nonradiolabeled SOD1−POx was coinjected with radiolabeled samples into the jugular vein. Blood and brain were collected at 60 min after iv injection as described previously and processed. Results were interpreted as brain/serum ratios.

2.11.5. Enzymatic Stability. To determine the presence of intact ^{125}I-SOD1−POx in serum and brain, samples were collected at 15, 60, and 240 min post iv injection and immediately used for TCA precipitation. Thereafter, the mouse was decapitated and the whole brain was removed, weighed, and placed in an ice-cold glass homogenizer. The brain was homogenized (10 strokes) in sodium phosphate buffer and then centrifuged at 5400*g* for 10 min. Brain supernatant was transferred to a new tube and mixed with an equal amount of 30% TCA. To correct for ex vivo degradation, processing control samples were prepared by adding 10,000 cpm of ^{125}I-SOD1−POx into serum or brains obtained from mice that had received no iv injection of radioactive material and processed similarly. All the TCA precipitated samples were then centrifuged at 5400*g* for another 10 min, and the supernatant and pellet were collected for radioactivity measurement. The stability was estimated by the percentage of radioactivity present in the pellet divided by the total radioactivity in both the pellet and the supernatant and then normalized by the percent of processing control. In some cases, a brain washout was performed prior to brain collection as described previously.

2.11.6. Capillary Depletion. Brain washout was performed at 60 min after iv injection of ^{125}I-SOD1−POx. This procedure removed the radioactively labeled material in the vascular space and loosely adhering to the luminal side of brain capillaries. Thereafter, the mouse was decapitated and the whole brain was removed, weighed, and homogenized (10 strokes) in physiological buffer (10 mM HEPES, 141 mM NaCL, 4 mM KCl, 2.8 mM CaCl$_2$, 1 mM MgSO$_4$, 1 mM NaH$_2$PO$_4$, and 10 mM D-glucose, pH 7.4). Dextran solution was added to the homogenate, mixed, and homogenized a second time (3 strokes). The homogenate was centrifuged at 5400*g* for 15 min at 40 °C. The resulting supernatant (brain parenchyma fraction) and pellet (capillary fraction) were separated, and the level of radioactivity for each fraction was determined using a γ-counter. The parenchyma/serum and capillary/serum ratios (μL/g) were calculated as (cpm/g of tissue)/(cpm/μL of serum).

2.11.7. Tissue Distribution. Mice anesthetized with urethane received an iv injection of 0.2 mL of LR-BSA containing both ^{131}I-SOD1 and ^{125}I-SOD1−POx (300,000 cpm of each) into the jugular vein. In a separate group, ^{131}I-albumin (300,000 cpm) was iv injected similarly. Blood from the carotid artery

was collected at 60 min after injection, mice were immediately decapitated, and brain, heart, liver, spleen, kidney, lung, stomach, and tight muscle were removed and weighed. The arterial blood was centrifuged at 5400*g* for 10 min, and the serum was collected. The radioactivity of tissue and serum samples was counted using a γ-counter. The tissue/serum ratios of ^{131}I-SOD1 and ^{125}I-SOD1−POx in each tissue were statistically compared (paried *t* test, *n* = 5).

2.12. Statistical Analysis. Statistical analysis was done using Student's *t* test for two groups and one-way ANOVA for multiple groups followed by Newman−Keuls multiple comparison test or by a 2-tailed unpaired *t* test with Welch's correction. A minimum *p* value of 0.05 was estimated as the significance level. Statistic analysis was done with the Prism 5.0 software (GraphPad, San Diego, CA, USA).

3. RESULTS

3.1. Synthesis and Characterization of SOD1−POx. Two well-defined block copolymers, P(MeOx-*b*-BuOx) and P(EtOx-*b*-BuOx) (Figure 1 and Table 1), were conjugated via

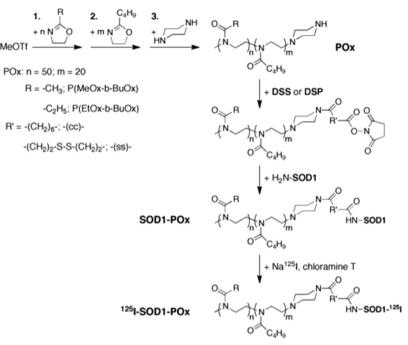**Table 1. Molecular Characteristics of Synthesized POx Block Copolymers**

polymer	M_n $(\times10^3)^a$	M_w $(\times10^3)^b$	M_n $(\times10^3)^b$	Đ^b	yield $(\%)^c$
P(EtOx$_{50}$-*b*-BuOx$_{20}$)	7.6	10.8	9.7	1.11	59
P(MeOx$_{50}$-*b*-BuOx$_{20}$)	6.8	10.2	8.2	1.25	89

^{a}Determined by end group analysis based on ^{1}H NMR spectroscopy data. ^{b}Determined by GPC. ^{c}Recovered yield.

the secondary amine function of the piperazine terminus of the polymers with SOD1 following a method we described previously. The synthesis for POx and SOD1−POx conjugates is outlined in Scheme 1. First, the polymers were reacted with bifunctional linkers DSS or DSP to produce *N*-hydroxysuccinimide terminated derivatives. Second, these activated polymers were reacted with SOD1 in an aqueous buffer (pH 8.0). To minimize the loss of SOD1 activity no organic solvent was added during this second step. The reactions proceeded readily and generated SOD1−POx conjugates with either a stable linker or a degradable linker, which are denoted herein as "-(cc)-" and "-(ss)-", respectively. Table 2 summarizes the abbreviated names of the conjugates along with their molecular characteristics and catalytic activity. The conjugates were purified by FPLC to remove nonmodified proteins and excess of polymer. The yield of the POx−SOD1 conjugation varied slightly from 30 to 50% as per initial SOD1.

The SOD1−POx conjugates were analyzed by SEC, MALDI-TOF MS, and SDS−PAGE. The conjugates eluted in a broad peak with a maximum having a shorter elution time around 7.5 min as compared to 8.1 min for the native SOD1 (Figure S1 in the Supporting Information). The main peak also contained a more rapidly eluting "shoulder" around 6−6.5 min, which can

Scheme 1. Schematic Representation of the Synthesis of Poly(2-oxazoline) (POx), the Conjugation of POx with SOD1, and the Radiolabeling of SOD1−POx[a]

[a]The details of POx synthesis has been reviewed elsewhere.[28] For SOD1−POx conjugation, first, piperazine-terminated amphiphilic POx copolymers were functionalized with a stable (DSS) or redox labile linker (DSP) to yield N-hydroxysuccinimide terminated POx. Second, the reactive POx were conjugated with the primary amines of SOD1 to yield SOD1−POx conjugates. SOD1−POx was radioactively labeled using the chloramine-T method for in vivo study.

Table 2. Molecular Characteristics of SOD1−POx Conjugates

conjugates[a]	linker	modification degree[b]	residual act. (% unmodified)[c]	T_m (°C)[d,e]
SOD1-(cc)-P(MeOx-b-BuOx)	DSS	2.2	36	88.65
SOD1-(ss)-P(MeOx-b-BuOx)	DSP	3.5	47	N/A
SOD1-(cc)-P(EtOx-b-BuOx)	DSS	2.5	34	88.38
SOD1-(ss)-P(EtOx-b-BuOx)	DSP	2.3	31	N/A

[a]Here "-(cc)-" and "-(ss)-" designate SOD1−POx conjugates containing stable and degradable bonds formed by DSS and DSP, respectively. [b]Counting per SOD1 dimer as determined by TNBS assay. [c]Determined by pyrogallol auto-oxidation assay. [d]Determined by DSC. [e]T_m of unmodified SOD1 is 92.14 °C.

be ascribed to highly modified protein fractions. In addition, a minor faction (ca. 3 to 5% of the total protein) rapidly eluting at 5.5 min was found in all conjugate samples, probably due to aggregation of highly modified protein. The MALDI-TOF mass spectrum (Figure 2) suggests that while the native SOD1 contained a mixture of a protein monomer (16 kDa) and a dimer (32 kDa), the SOD1−POx conjugates represented mainly a dimer with one (39 to 40 kDa) or two (46−48 kDa) polymer chains attached. In addition the conjugate samples also contained some unmodified SOD1 monomer and dimer, which probably originated from the native enzyme not participating in the reaction or from degradation during sampling. It should be pointed out that MALDI-TOF MS may not detect the highly modified protein conjugates due to the mass bias of the method, which can be still present in the mixture similar to

PEGylated SOD1.[39] Such highly modified conjugates appeared in the SDS−PAGE, which revealed the existence of multiple protein forms in all SOD1−POx samples, including a major band of a modified dimer and several smaller bands of higher molar mass (Figure 3). The latter bands may contain SOD1 with multiple polymer chains attached. This assumption is corroborated by the mean modification degree of the conjugates determined by TNBS amino group titration assay (Table 2). Here, the degree of modification varied from ca. 2.2 for SOD1-(cc)-P(MeOx-b-BuOx) to 3.5 for SOD1-(ss)-P(MeOx-b-BuOx) per SOD1 dimer. The residual enzymatic activities of SOD1−POx conjugates as determined by the pyrogallol auto-oxidation assay were found to be around 30% for SOD1-(ss)-P(EtOx-b-BuOx) and 47% for SOD1-(ss)-P(MeOx-b-BuOx) as compared to native SOD1 (Table 2). Others reported a similar activity loss (down to ca. 50%) for PEGylated SOD1.[40] It was consistent with previous findings that modification of SOD1 lysines, such as acylation and carbamoylation, decreases electrostatic attraction of the super-oxide anion to the enzyme active site.[11,41] As SOD1-(cc)-POx and SOD1-(ss)-POx are very similar in terms of their degree of modification as well as their residual activities, we selected both SOD1-(cc)-P(MeOx-b-BuOx) and SOD1-(cc)-P(EtOx-b-BuOx) for further studies.

3.2. Protein Stability and Aggregation of SOD1−POx. The impact of POx conjugation (POxylation) on the stability of SOD1 was investigated by circular dicroism (CD) and differential scanning calorimetry (DSC). The CD signals of SOD1−POx conjugates in the far-UV are practically identical to those for native SOD1, suggesting that the secondary structure of the protein remained unaffected by the POxylation (Figure 4). Native SOD1 and SOD1−POx conjugates displayed a single
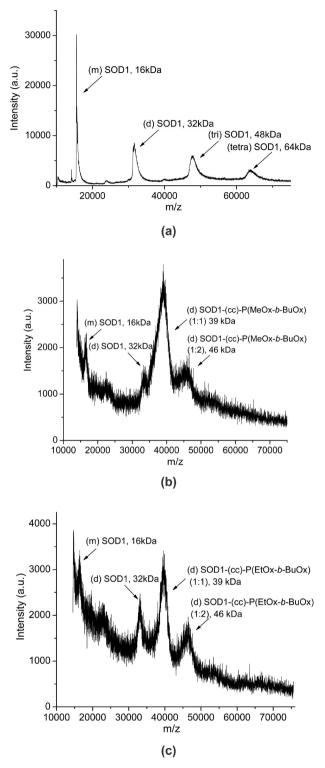
Figure 2. Representative MALDI-TOF MS of (a) SOD1, (b) SOD1-(cc)-P(MeOx-*b*-BuOx), and (c) SOD1-(cc)-P(EtOx-*b*-BuOx). The average molar mass and composition of each peak are labeled. (m) SOD1, SOD1 monomer; (d) SOD1, SOD1 dimer; (tri) SOD1, SOD1 trimer; (tetra) SOD1, SOD1 tetramer.
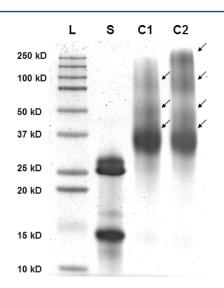

Figure 3. Representative SDS−PAGE of SOD1 and SOD1−POx: L, ladder; S, SOD1; C1, SOD1-(cc)-P(MeOx-*b*-BuOx); C2, SOD1-(cc)-P(EtOx-*b*-BuOx). The conjugates are marked by arrows.
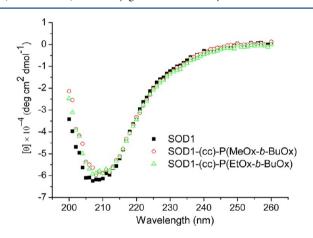

Figure 4. Representative far-UV CD spectra of SOD1 and SOD1−POx. All samples were dissolved in PBS (pH 7.4) at 0.5 mg/mL as determined by MicroBCA assay.

endothermal peak in the DSC melting curves (Figure S2 in the Supporting Information), and the T_m values of SOD1−POx conjugates were decreased by only ca. 3.5 °C as compared to the native protein (T_m = 92.1 °C) (Table 2). Thus, the SOD1−POx conjugates and unmodified enzyme have a similar thermal stability. The aggregation of SOD1−POx conjugates in buffer solution was analyzed by DLS. Using the volume-based size distributions, some increases in the particle effective diameters were observed for both SOD1−POx conjugates as compared to the native SOD1 (ca. 5 nm) (Figure 5). Interestingly, the SOD1-(cc)-P(EtOx-*b*-BuOx) conjugate formed larger aggregates (ca. 20 nm) than SOD1-(cc)-P(MeOx-*b*-BuOx) (ca. 8 nm). This can be attributed to the slightly amphiphilic nature of the still water-soluble EtOx-block.[42,43] All studied solutions including native SOD1 contained minor amounts of larger aggregates, which were more evident in the analysis of the intensity-based size distributions (Figure S3 in the Supporting Information).

3.3. Neuronal Cell Toxicity and Trafficking of SOD1−POx. The cellular interactions of SOD1−POx conjugates were studied using CATH.a neurons as an in vitro model of neuronal cells. The unmodified SOD1 and SOD1−PEG conjugate were used for comparison. The exposure of cells to 80 μg/mL of native or POxylated SOD1 for 1 to 24 h did not result in a considerable cytotoxic effect (Figure 6), whereas the exposure to 100 μg/mL of cationic PEG-*b*-PLL used herein as a positive control generated a significant time-dependent cytotoxicity.
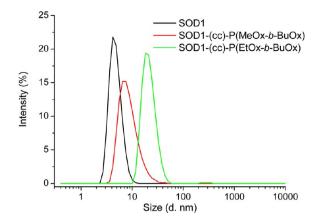
Figure 5. Volume-based size distributions of the particles in SOD1 and SOD1−POx solutions determined by DLS at 25 °C. All samples were dissolved in PBS (pH 7.4) at 0.5 mg/mL and sterile filtered (450 nm filter) prior to the measurements.
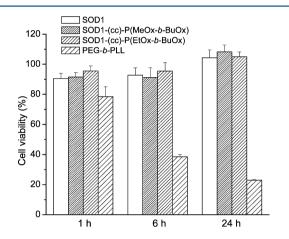

Figure 6. Cytotoxicity of SOD1, SOD1−POx, and PEG5000-b-PLL$_{50}$ in CATH.a neuronal cells. Cells were incubated with 80 μg/mL of SOD1 or SOD1−polymer conjugates for 1 h, 6 h, or 24 h in full medium and were allowed to grow for another 48 h. Cytotoxicity was determined by the cell counting assay. Data are means ± SEM ($n = 6$).

The uptake of SOD1, SOD1−PEG, and SOD1−POx in the CATH.a neurons was analyzed at different time points by measuring the SOD1 concentration in the cell lysates using ELISA. Neither unmodified SOD1 nor SOD1−PEG exhibited any uptake for up to 24 h within the detection limit of the method (ca. 0.5 ng/mL, which allows detection of 0.2 ng of SOD1/mg of the cellular protein). In contrast, both SOD1−POx conjugates were readily taken up by the cells in a time-dependent manner during 24 h (Figure 7a). Interestingly, the SOD1-(cc)-P(EtOx-b-BuOx) conjugate showed 4- to 7-fold higher uptake rate and levels as compared to the SOD1-(cc)-P(MeOx-b-BuOx) conjugate. The cellular uptake of SOD1-(cc)-P(EtOx-b-BuOx) during the first 6 h reached as much as 30 ng/mg cell protein. The ELISA data were further corroborated by a CLSM study using Alexa Fluor 647 labeled SOD1 and SOD1−POx conjugates. This study confirmed a considerable increase in the internalization rate of the conjugates as compared to the native enzyme as well as a clear intracellular localization of the conjugates in CATH.a cells (Figure 7b). Notably, CLSM revealed a similar trend in the uptake of the SOD1-(cc)-P(EtOx-b-BuOx) and SOD1-(cc)-P(MeOx-b-BuOx) conjugates, suggesting that a slightly more hydrophobic EtOx block enhances the internalization of the

POxylated SOD1 in the cells (Figure S4 in the Supporting Information). Based on the ELISA and CLSM cellular uptake data we selected SOD1-(cc)-P(EtOx-b-BuOx) as the lead compound for the further studies.
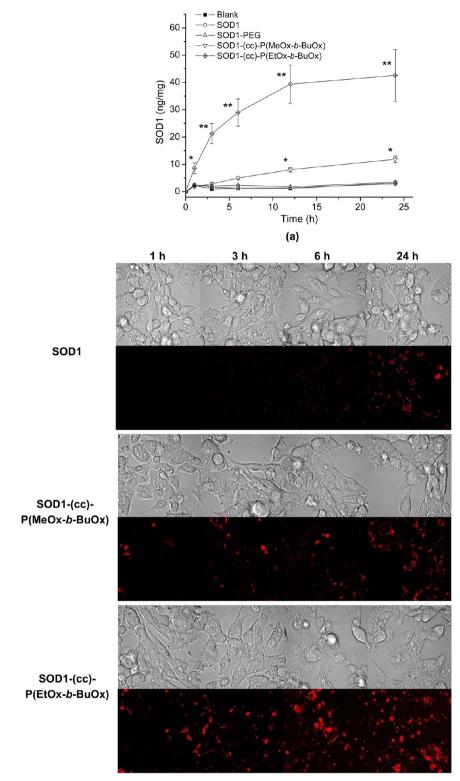
First, the subcellular distribution of the SOD1-(cc)-P(EtOx-b-BuOx) conjugate was examined. Using organelle-specific fluorescent dyes we observed different extents of colocalization of this conjugate with the nucleus, lysosomes, mitochondria, and ER (Figure 8a). As indicated from quantitative analysis of the colocalization data after 6 h incubation with SOD1-(cc)-P(EtOx-b-BuOx), the conjugate was mainly observed in the ER (41 ± 3.2%) and mitochondria (21 ± 1.6%) (Figure 8b). The fractions found in the lysosomes (10 ± 1.7%) and the nucleus (5.6 ± 0.31%) were considerably smaller.

Second, the cell entry mechanism of SOD1-(cc)-P(EtOx-b-BuOx) conjugate was examined by inhibition of the clathrin-mediated endocytosis (CME) and the lipid raft/caveolae-mediated endocytosis pathways. The hypertonic sucrose and MBCD are the commonly used chemical inhibitors for these pathways.[34] We have shown that, in our cell model, these inhibitors indeed decreased the internalization of the protein markers for the respective pathways: Tf for clathrin and CTB for caveolae (Figure S5 in the Supporting Information). Interestingly, after coexposure of the CATH.a cells to each of these markers with the SOD1-(cc)-P(EtOx-b-BuOx) conjugate, colocalization of the conjugate with CTB (25 ± 2.3%) was found to be significantly higher than its colocalization with Tf (9.3 ± 0.40%) (Figures 8c and 8d). Furthermore, the uptake of the conjugate was inhibited significantly by MBCD ($p < 0.01$) but not by hypertonic sucrose, suggesting that the conjugate is internalized through lipid raft/caveolae rather than CME (Figure 8e and Figure S6 in the Supporting Information). Very similar colocalization and inhibition patterns were also observed for the P(EtOx-b-BuOx) block copolymer alone (Figures S7 and S8 in the Supporting Information), suggesting that the SOD1−POx conjugate may follow the trafficking itinerary of POx used for the conjugation.

3.4. Intracellular Superoxide Scavenging by SOD1−POx. The activity of SOD1-(cc)-P(EtOx-b-BuOx) after cell uptake was quantified by the luminol-based chemiluminescence assay (Figure 9). This assay employs the superoxide-generation system, HX-XO, and luminol, which reacts with the superoxide and emits a strong chemiluminescence signal. This signal can be completely abolished by depleting the superoxide with 4 kU/mL of SOD1 or partially abolished with 0.4 kU/mL of SOD1, indicating that the detected signal is superoxide-dependent (Figure S9 in the Supporting Information). The cell lysate (blank control) was shown to significantly decrease the chemiluminescence signal compared to the control. This is likely to be due to the presence of endogenous superoxide dismutases and other superoxide scavengers in CATH.a cells (Figure 9a). The scavenger activity in these cells was considerably increased after their treatment with SOD1-(cc)-P(EtOx-b-BuOx), which was consistent with the accumulation of the active enzyme in the cell lysates. In contrast, the scavenging activity did not change significantly after the treatment of the cells with native SOD1 or PEGylated SOD1. A time lapse experiment clearly showed that the significant reduction in superoxide after treatment with SOD1-(cc)-P(EtOx-b-BuOx) translates into a much smaller area under the curve for the superoxide concentration (Figure 9b).

Finally, the ability of SOD1, SOD1−PEG, and SOD1-(cc)-P(EtOx-b-BuOx) to attenuate the Ang II-induced increase in

(a)

(b)

Figure 7. (a) Cellular uptake of SOD1, SOD1−PEG, and SOD1−POx in CATH.a neuronal cells. Cells were incubated with 80 μg/mL of SOD1 or SOD1−polymer conjugates for 1 to 24 h in serum-free medium. Total cellular uptake was determined by SOD1 ELISA and normalized to the total cell protein determined by MicroBCA assay. Data are means ± SEM ($n = 3$), *$p < 0.05$ and **$p < 0.01$. (b) Cellular uptake of fluorescently labeled SOD1 and SOD1−POx obtained by CLSM. Cells were incubated with 80 μg/mL of SOD1 or SOD1−POx for 1−24 h in serum-free conditions and imaged by CLSM.

intracellular superoxide levels in CATH.a cells was determined by EPR spectroscopy (Figure 10). A 30 min Ang II stimulation increased the superoxide levels as determined by an increase in

the EPR spectrum amplitude. A pretreatment of neurons with SOD1-(cc)-P(EtOx-b-BuOx) resulted in a decrease of this signal (Figure 10b), suggesting that this conjugate mitigated the
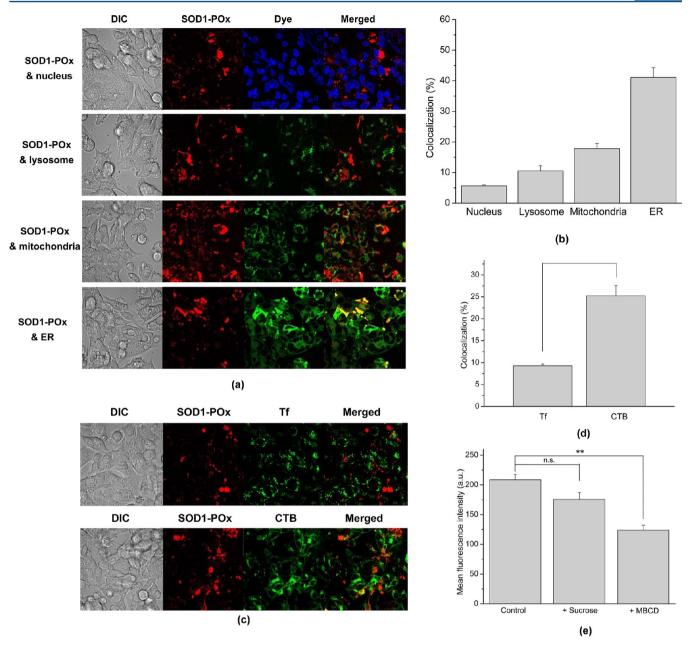
Figure 8. Intracellular distribution and endocytosis of fluorescently labeled SOD1−POx in CATH.a neuronal cells. (a) Intracellular distribution of SOD1-(cc)-P(EtOx-*b*-BuOx). Cells were incubated with 80 μg/mL of SOD1-(cc)-P(EtOx-*b*-BuOx) for 6 h and stained with Hoechst 33342, MitoTracker, LysoTracker, or ER-Tracker for 30 min. (b) Quantitative colocalization analysis of SOD1-(cc)-P(EtOx-*b*-BuOx) with organelle-specific dyes. (c) Colocalization of SOD1-(cc)-P(EtOx-*b*-BuOx) with specific endocytosis markers Tf and CTB. Cells were coincubated with 80 μg/mL of SOD1-(cc)-P(EtOx-*b*-BuOx) and Alexa Fluor 488-conjugated Tf or CTB for 6 h. (d) Quantitative colocalization analysis of SOD1-(cc)-P(EtOx-*b*-BuOx) with Tf and CTB. (e) Inhibition of the cellular uptake of SOD1-(cc)-P(EtOx-*b*-BuOx) by hypertonic sucrose and MBCD as determined by CLSM. Cells were pretreated with hypertonic 0.4 M sucrose or 4 mM MBCD for 30 min and then coincubated with 80 μg/mL of SOD1-(cc)-P(EtOx-*b*-BuOx) for 6 h. The quantitative mean fluorescence intensity was analyzed and compared with nontreated controls. Data are presented as means ± SEM ($n = 10-15$), **$p < 0.01$.

Ang II-induced increase in superoxide level. As expected, the treatment of the cells with native SOD1 failed to attenuate the response to Ang II stimulation. PEGylated SOD1 had some antioxidant activity as judged by the decreased EPR signal albeit it was significantly less than the effect observed for POxylated SOD1. Altogether, the POxylation of SOD1 results in an enhanced transport of the enzyme into CATH.a neuronal cells and allows significant scavenging of intracellular superoxide generated in response to Ang II stimulation.

3.5. Pharmacokinetics, Brain Uptake, and Tissue Distribution of ^{125}I-SOD1−POx. The animal studies were conducted with a radiolabeled SOD1-(cc)-P(EtOx-*b*-BuOx) conjugate prepared by the chloramine-T method (Scheme 1). To confirm the successful iodination, we analyzed radioactively labeled POxylated SOD1 by autoradiograph gel (Figure S10 in the Supporting Information). At the electrophoresis conditions, SOD1 presented as a mixture of dimer and monomer (lane A). ^{125}I-SOD1−POx showed a similar pattern (lanes B and C), confirming that the conjugate retained its structure after
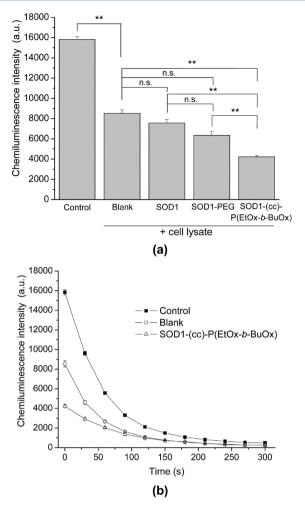
(a)

(b)

Figure 9. Intracellular SOD activity of SOD1, SOD1−PEG, and SOD1-(cc)-P(EtOx-*b*-BuOx) in CATH.a neuronal cells. Cells were incubated with 80 μg/mL of SOD1 or SOD1−polymer conjugates for 12 h in serum-free conditions. SOD activities of the treated and nontreated cell lysate were determined by luminol-based chemiluminescence assay. HX-XO system was used as the superoxide source. (a) Chemiluminescence signals of the tested samples immediately after mixing of reagents and cell lysates or buffer (for control). Data are presented as means ± SEM ($n = 3$), **$p < 0.01$. (b) Representative curves of the time decay of the chemiluminescence after mixing for the control, nontreated (blank), and SOD1-(cc)-P(EtOx-*b*-BuOx)-treated cell lysate.

iodination and the samples injected into animals for PK studies were of the same composition as those used in nonradioactive experiments.

In Figure 11a the serum concentrations of ^{125}I-SOD1 or ^{125}I-SOD1-(cc)-P(EtOx-*b*-BuOx) are plotted against time and compared to coinjected ^{131}I-albumin. The initial volume distribution ($V_{t(0)}$) for ^{131}I albumin was 1.95 ± 0.02 mL (SOD1−POx group) or 2.12 ± 0.03 mL (SOD1 group). The elimination half-time of ^{131}I albumin was determined to be 3.87 h (SOD1−POx group) or 3.50 h (SOD1 group), which is consistent with the results previously found,[44,45] and suggests that we have successfully estimated the pharmacokinetic profiles of ^{125}I labeled sample and ^{131}I-albumin in these animals. Both samples showed biphasic clearance from serum (Figure 11a); during the initial phase (0−60 min) (Figure 11b), the calculated half-time disappearance of SOD1−POx was about 2 times longer as compared to the native protein (28.4 vs
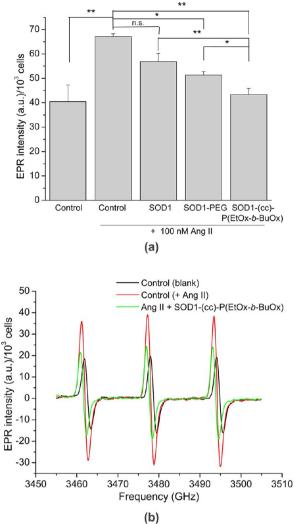

(a)

(b)

Figure 10. Intracellular superoxide scavenging of SOD1, SOD1−PEG, and SOD1-(cc)-P(EtOx-*b*-BuOx) in CATH.a neuronal cells. Cells were incubated with 80 μg/mL of SOD1 or SOD1−polymer conjugates for 12 h in serum-free conditions. CMH was added as the cell-permeable, superoxide-sensitive spin probe. Superoxide was generated by stimulating neurons with 100 nM Ang II. CMH radical signal was recorded by EPR spectroscopy and normalized to total cell number. (a) Normalized EPR signals of the tested samples. Data are presented as means ± SEM ($n = 3$), *$p < 0.05$ and **$p < 0.01$. (b) Representative normalized EPR spectra of the negative control (blank), positive control (with Ang II), and SOD1-(cc)-P(EtOx-*b*-BuOx) treated cells.

15.9 min). The initial volumes of distribution of SOD1−POx and SOD1 in blood were 1.47 ± 0.03 mL and 1.78 ± 0.03 mL, respectively.

In Figure 12a,b, the brain/serum ratio of labeled native and POxylated SOD1, corrected by the brain/serum ratio for the coinjected ^{131}I-albumin, is plotted against exposure time to calculate the blood-to-brain influx rate (this allows us to correct results for each animal for its vascular space and thus more accurately estimate the results). The slope, K_i, of the linear portion (0−60 min) of the albumin-corrected plot was 0.052 ± 0.006 μL/g·min ($r = 0.86$, $p < 0.0001$; $n = 1−2$ mice/time point) for ^{125}I-SOD1−POx, demonstrating that the substance crossed the BBB significantly faster than albumin. In comparison, no correlation was observed for ^{125}I-SOD1 that
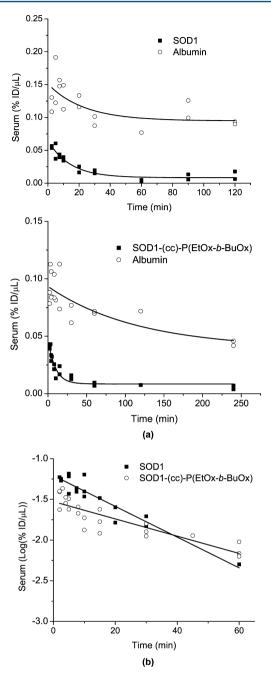
(a)

(b)

Figure 11. PK of radiolabeled SOD1 and SOD1-(cc)-P(EtOx-*b*-BuOx) in mice. (a) Serum clearance of ^{125}I-SOD and ^{125}I-SOD-(cc)-P(EtOx-*b*-BuOx) with coinjected ^{131}I-albumin following iv injection. (b) The initial distribution phase (0−60 min) of ^{125}I-SOD1 and 125I-SOD1-(cc)-P(EtOx-*b*-BuOx) after injection was linear, and the half-time disappearance from blood was 28.39 min for SOD1-(cc)-P(EtOx-*b*-BuOx) and 15.94 min for SOD1. The clearance of SOD1 is significantly faster than that of SOD1-(cc)-P(EtOx-*b*-BuOx) (*p* < 0.001).

does not cross the BBB any better than albumin. The initial volume of distribution in brain for SOD1−POx was 2.12 ± 0.05 μL/g. By 4 h post iv injection, the amount of ^{125}I-SOD1−POx taken up by the brain reached a maximum value of 0.08% ID/g (Figure 12c). Notably, the brain uptake of SOD1−POx was not saturable, as the brain/serum ratio of ^{125}I-SOD1−POx was not inhibited by an excess amount of coinjected nonradioactive SOD1−POx (Figure 12d).

The in vivo stability of ^{125}I-SOD1−POx in serum and brain was measured by TCA precipitation (Table S1 in the Supporting Information). Following iv injection, the intact ^{125}I-SOD1−POx present in serum was determined to be about 104% at 15 min, 99% after 1 h, and 77% at 240 min; whereas in brain the intact ^{125}I-SOD1−POx was about 97% at 15 min, 84% at 60 min, and 44% after 240 min. More than 50% of intact ^{125}I-SOD1−POx was observed in the brain for animals receiving brain washout at 1 h post iv injection. These results indicate that SOD1−POx is stable in serum and brain for over 1 h after iv administration.

To determine whether ^{125}I-SOD1−POx was sequestered by brain endothelial cells or entered into the brain parenchyma space, capillary depletion with brain washout was performed in mice 1 h after iv injection. As shown in Figure 12e, the brain parenchyma/serum ratio was found to be significantly higher as compared to the capillary/serum ratio (5.56 ± 0.97 μL/g vs 2.78 ± 0.40 μL/g, *p* < 0.05; *n* = 3 mice). This indicates that SOD1−POx can cross the BBB completely and enter the brain's parenchyma space.

The tissue/serum ratios of ^{125}I-SOD1−POx accumulation in peripheral tissues (heart, liver, spleen, kidney, lung, muscle, and stomach) at 60 min after iv injection were determind (Figure 13). ^{131}I-SOD1 was coinjected and used as control. The tissue/serum ratio of SOD1−POx in brain, heart, liver, spleen, and lung were all significantly higher than that of SOD1 (*p* < 0.05, *n* = 5), whereas in kidney, muscle, and stomach no significant difference could be observed.

4. DISCUSSION

In the present study, we successfully modified SOD1 with two amphiphilic POx block copolymers and evaluated the cellular uptake and therapeutic potential of these conjugates. These SOD1−POx conjugates were synthesized by a two-step conjugation method. In order to avoid protein denaturation and to preserve a higher residual enzymatic activity the conjugation was performed in aqueous medium with no added organic cosolvents.[46] The recovered yields (30−50% as per initial amount of SOD1) are comparable to those reported before for the preparation of HRP−POx conjugates (20−40%).[25] The POxylated SOD1 could be readily purified, and its analysis by SEC, MALDI-TOF MS, SDS−PAGE, and TNBS assay showed that the conjugates contained 2−3 POx chains per protein dimer. The secondary structure of SOD1 was preserved as revealed by CD spectroscopy, and no significant SOD1 dimer dissociation was observed. DSC analysis showed that POxylation of SOD1 did not result in a destabilization of the enzyme. These results indicated that SOD1−POx conjugates maintained high conformational and thermal stability, which is crucial for future manufacturing and clinical applications. However, we observed a catalytic activity loss with a residual activity of 30−40% similar to SOD1−Pluronic conjugates prepared in the same way.[9] This suggests that the lysine modification, rather than conformational changes or dimer dissociation of SOD1, is accountable for the activity loss of the enzyme. Consequently, the loss of the enzyme activity is proportional to the degree of modification and is adjustable by altering the conjugation conditions. For example, the heavily modified SOD1−POx conjugates with an average of 5 to 6 conjugated polymers exhibited only 5% of its original activity (data not shown). Interestingly, when using PMeOx and PEtOx homopolymers for enzyme modification, the former exhibited a higher influence on the residual enzymatic activity as compared
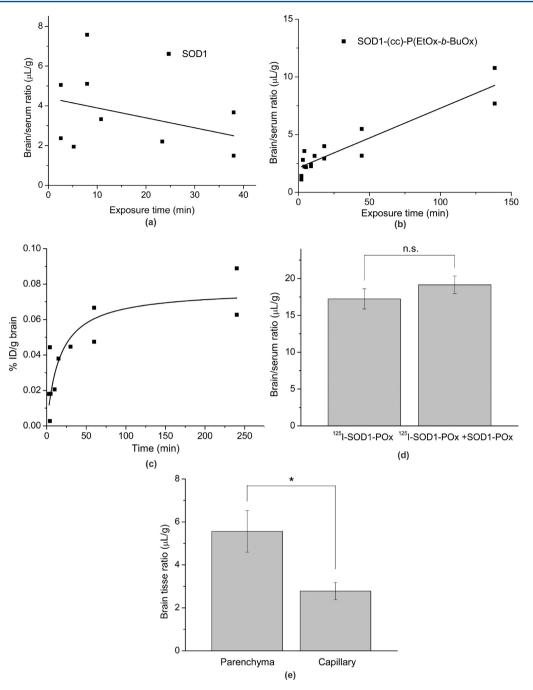
Figure 12. BBB transport and brain uptake of radiolabeled SOD1-(cc)-P(EtOx-*b*-BuOx) in mice. (a, b) Multiple-time regression analysis of (a) ^{125}I-SOD1 and (b) ^{125}I-SOD1-(cc)-P(EtOx-*b*-BuOx) transport across the BBB. ^{131}I-albumin was coinjected in each group, and the brain serum ratio of ^{131}I-albumin was subtracted from that of ^{125}I-SOD1 or ^{125}I-SOD1-(cc)-P(EtOx-*b*-BuOx) to correct the vascular space of each individual animal. For SOD1−POx, the unidirectional influx rate, $K_i = 0.052 \pm 0.006$ μL/g·min; vascular distribution, $V_{i(0)} = 2.121 \pm 0.05$ μL/g ($r = 0.86$, $p < 0.0001$; $n = 1−2$ mice/time point). In comparison, there was no linear relation between the brain/serum ratio of SOD1 and its exposure time, indicating no entry of SOD1 into the brain. (c) Brain uptake of ^{125}I-SOD1-(cc)-P(EtOx-*b*-BuOx) following iv injection. The results were corrected for the distribution volume in the brain of SOD1−POx at $t = 0$. The maximal value after 4 h following iv injection was estimated by a one-site binding model to approach 0.08% ID/g. (d) Nonradioactive SOD1-(cc)-P(EtOx-*b*-BuOx) (5 μg/mouse) did not inhibit the brain/serum ratio of [125]I-(cc)-P(EtOx-*b*-BuOx) at 60 min after iv injection. No statistically significant difference was observed between animals receiving ^{125}I-SOD1−POx and animals receiving ^{125}I-SOD1−POx plus SOD1−POx ($n = 7$). (e) Distribution of ^{125}I-SOD1-(cc)-P(EtOx-*b*-BuOx) in brain parenchyma and capillary fractions. The vascular space was washed free of blood at 60 min following iv injection. The brain parenchyma/serum ratio was significantly higher than the capillary/serum ratio (5.56 $\pm$ 0.97 μL/g vs 2.78 $\pm$ 0.40 μL/g) (*$p < 0.05$; $n = 3$).

to the latter.[47,48] Here, we observed a contrary trend. The conjugates prepared in the present study were moderately modified, bearing on average 2−3 polymers per enzyme, and retained a relatively high residual activity.

Aggregation is a major issue for the development of therapeutic proteins. It is reported that chemical degradation or modification can induce partial protein unfolding and irreversible protein aggregation.[49,50] The aggregation behavior of POxylated SOD1−POx as studied by DLS showed, in both
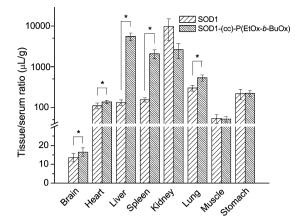
Figure 13. Tissue distribution of ^{125}I-SOD1-(cc)-P(EtOx-*b*-BuOx) and coinjected ^{131}I-SOD1 at 60 min following iv injection. Results were interpreted as tissue/serum ratio in μL per gram of tissue ($n = 5$). The tissue/serum ratio of SOD1−POx in brain, heart, liver, spleen, and lung were all significantly higher than that of SOD1 (* $p < 0.05$), whereas for kidney, muscle, and stomach no significant difference was observed.

intensity-based and volume-based size distributions, a significant increase of the hydrodynamic size of aggregates as compared to the native SOD1. SEC profiles indicated that a small fraction (3−5%) of large size aggregates are formed. The increased aggregation of SOD1−POx is probably due to the self-association of hydrophobic blocks (BuOx) of POx exposed on the surface of proteins and thus is likely to be reversible. It did not result in protein unfolding and conformation change, as no enzyme denaturation could be detected. However, its effect on the long-term physical and chemical stability of SOD1 is unclear and calls for further investigations.

The motivation for POxylation of hydrophilic proteins is to enhance the cellular binding and uptake of the protein.[29] In the present study we evaluated the cellular delivery of POxylated SOD1 in CATH.a neuron cells. SOD1−POx conjugates did not generate a detectable neuronal toxicity at the concentration of 80 μg/mL. Enhanced neuronal uptake of SOD1−POx was found by both SOD1 ELISA and fluorescent quantification. Interestingly, SOD1−P(EtOx-*b*-BuOx) exhibited a much better cell uptake as compared to SOD1−P(MeOx-*b*-BuOx), whereas in our previous study, HRP−P(MeOx-*b*-BuOx) showed higher uptake than that of HRP−P(EtOx-*b*-BuOx) in both MDCK and Caco-2 cells.[25] The variance in the modification degree and/or formation of different aggregates for both systems is probably one reason for the different behavior of the two POxylated proteins. Moreover, HRP−P(MeOx-*b*-BuOx) had a higher modification degree than that of SOD1−P(EtOx-*b*-BuOx) (1.62 vs 1.04), but for SOD1 modification, the modification degree of SOD1−P(EtOx-*b*-BuOx) in the cellular uptake study was higher (2.18 vs 2.49). For both conjugates, the neuronal uptake was slow and time-dependent. For SOD1−P(EtOx-*b*-BuOx), significant neuronal internalization was observed after 3 to 6 h treatment, as revealed by CLSM.

Previous studies have demonstrated that modification with amphiphilic block copolymers such as Pluronics and POx can enhance the cellular uptake of various proteins, however, little is known about their intracellular fate. We analyzed the intracellular distribution and endocytosis pathway of SOD1−P(EtOx-*b*-BuOx) in CATH.a neurons. Our data suggested that SOD1−P(EtOx-*b*-BuOx) mainly utilizes lipid raft/caveolae-

mediated endocytosis to internalize into CATH.a neurons, which is similar to the internalization of the polymer alone. SOD1−P(EtOx-*b*-BuOx) may also utilize caveolae and clathrin-independent pathways, which also require lipid raft compositions and can be inhibited by cholesterol depletors such as MBCD.[33,51,52]

Colocalization studies indicate that SOD1−P(EtOx-*b*-BuOx) is not entrapped in lysosomes but accumulates in the ER and to a lesser extent in mitochondria after cell entry. This result corroborates that SOD1−POx used clathrin-independent endocytosis pathways as these pathways often do not involve lysosome trafficking.[33,51] It also suggests that SOD1−POx conjugates should maintain high intracellular activity because they are not trapped and degraded in lysosomes. Interestingly, high colocalization with mitochondria was observed (ca. 18% after 6 h treatment), suggesting that SOD1−P(EtOx-*b*-BuOx) can be transported to mitochondria after endocytosis and thus is able to scavenge the intercellular superoxide generated in this organelle, which is one of the major sources of intracellular ROS.[53] Chemiluminescence assay also confirmed that internalized SOD1−POx were catalytically active even after 12 h.

Ang II stimulation can induce an increase of intraneuronal superoxide level produced by NADPH oxidases and/or mitochondria.[7] Our previous study showed that the SOD1−Pluronic conjugates can significantly attenuate the increase of superoxide in CATH.a neurons stimulated by Ang II.[9] In the present study, we demonstrated that SOD1−POx displayed the same capability by using EPR spectroscopy, which is widely accepted for intracellular free radical measurement.[54] The superoxide scavenging ability of SOD1−POx is clearly superior to native SOD1 and SOD1−PEG, which showed minimal uptake in CATH.a neurons. The high colocalization of SOD1−POx with mitochondria further reinforced its superoxide scavenging ability because Ang II stimulates the increase of superoxide in both cytoplasm and mitochondria. Our data indicates that SOD1−POx are promising candidates as efficient superoxide scavengers in neuronal cells. However, it should be noted that SOD1−POx alone is not sufficient to remove intracellular oxidative stress as it generates another type of ROS, hydrogen peroxide. A combination of SOD1−POx and a hydrogen peroxide scavenger (e.g., catalase−POx conjugate) might be a promising strategy to address this problem as indeed such combination systems have been successfully designed and reported recently.[55,56]

The half-life of SOD1-(cc)-P(EtOx-*b*-BuOx) in blood is about 1.75 times longer than that of native SOD1 (28 min vs 16 min), suggesting a slower elimination and increased circulation stability of this conjugate. However, this effect is not comparable to PEGylated SOD1, which results in a half-life of SOD1 of several to 24 h. The high accumulation of SOD1−POx in brain and other peripheral organs such as liver, spleen, and lung may be responsible for the observed shorter circulation time. Importantly, our data clearly showed that SOD1−POx is capable of crossing the intact BBB (entry rate of 0.052 ± 0.006 μL/g·min) and accumulating in both brain capillary and parenchyma (67% in parenchyma vs 33% in brain capillary), whereas, according to our and previous studies, neither native nor PEGylated SOD1 can reach the brain. This result is important as it indicates a direct therapeutic potential of POxylated SOD1 or other proteins for multiple CNS diseases with an intact BBB. Notably, even though SOD1−POx had a relatively short half-life, its portions retained in serum and in brain still maintained high structural stability (77% vs 84% at

1 h), indicating that SOD1−POx is not chemically degraded before or after crossing the BBB and thus most likely remains active when it reaches the target cells. The BBB transport of SOD1−POx was not inhibited by an excess of non-radioactively labeled conjugates, indicating that this transport employed a nonsaturable mechanism. The exact mechanism for the entry of SOD1−POx to the brain is unclear and needs further investigation, but it can be speculated that, similar to the observed endocytosis of SOD1−POx in CATH.a neurons, nonspecific transcytosis may play a role. As the synthesis of POx by living ionic polymerization allows a fine-tuning of the hydrophilic/lipophilic balance as well as the overall polymer architecture, optimization of the blood pool residence and trans-BBB transport might be possible. To address both possibly opposing properties, a better structure−property relationship for the POx as well as the protein−POx conjugates is needed. Related studies are currently in progress in our laboratories.

5. CONCLUSION

In the present study, a new type of SOD1−POx conjugate was synthesized, characterized, and evaluated in vitro and in vivo. SOD1−POx conjugates displayed low to no cytotoxicity and significantly enhanced neuronal uptake as compared to the native and PEGylated enzyme. The conjugate utilized caveolae-mediated and/or clathrin-independent and caveolae-independent endocytosis pathways, rather than the clathrin-medidated endocytosis to internalize into CATH.a neurons. The SOD1−POx maintained its catalytic activity after internalization. SOD1−POx significantly attenuated the increase of intracellular superoxide stimulated by Ang II. SOD1−POx showed two-times longer half-life in blood as compared to the native enzyme. Most importantly, SOD1−POx was able to cross the blood−brain barrier. Our results indicate that SOD1−POx conjugates might be promising polymer agents for antioxidant therapies of superoxide-related diseases in brain.

ASSOCIATED CONTENT

Ⓢ Supporting Information
Additional table and figures as discussed in the text. This material is available free of charge via the Internet at http://pubs.acs.org.

AUTHOR INFORMATION

Corresponding Author
*UNC Eshelman School of Pharmacy, University of North Carolina at Chapel Hill, Chapel Hill, NC 27599-7362. Tel: (919) 537-3800. Fax: (919) 962-9922E-mail: kabanov@email.unc.edu.

Author Contributions
§Both authors contributed equally to this work.

Notes
The authors declare no competing financial interest.

ACKNOWLEDGMENTS

REFERENCES

(1) Behl, C.; Moosmann, B. Oxidative nerve cell death in Alzheimer's disease and stroke: antioxidants as neuroprotective compounds. *Biol. Chem.* **2002**, *383*, 521−536.

(2) Halliwell, B. Reactive oxygen species and the central nervous system. *J. Neurochem.* **1992**, *59*, 1609−1623.

(3) Dhalla, N. S.; Temsah, R. M.; Netticadan, T. Role of oxidative stress in cardiovascular diseases. *J. Hypertens.* **2000**, *18*, 655−673.

(4) Zimmerman, M. C.; Davisson, R. L. Redox signaling in central neural regulation of cardiovascular function. *Prog. Biophys. Mol. Biol.* **2004**, *84*, 125−149.

(5) Welch, W. J. Angiotensin II-dependent superoxide: effects on hypertension and vascular dysfunction. *Hypertension* **2008**, *52*, 51−56.

(6) Zimmerman, M. C.; Sharma, R. V.; Davisson, R. L. Superoxide mediates angiotensin II-induced influx of extracellular calcium in neural cells. *Hypertension* **2005**, *45*, 717−723.

(7) Yin, J. X.; Yang, R. F.; Li, S.; Renshaw, A. O.; Li, Y. L.; Schultz, H. D.; Zimmerman, M. C. Mitochondria-produced superoxide mediates angiotensin II-induced inhibition of neuronal potassium current. *Am. J. Physiol.* **2010**, *298*, C857−C865.

(8) Rosenbaugh, E. G.; Roat, J. W.; Gao, L.; Yang, R. F.; Manickam, D. S.; Yin, J. X.; Schultz, H. D.; Bronich, T. K.; Batrakova, E. V.; Kabanov, A. V.; Zucker, I. H.; Zimmerman, M. C. The attenuation of central angiotensin II-dependent pressor response and intra-neuronal signaling by intracarotid injection of nanoformulated copper/zinc superoxide dismutase. *Biomaterials* **2010**, *31*, 5218−5226.

(9) Yi, X.; Zimmerman, M. C.; Yang, R.; Tong, J.; Vinogradov, S.; Kabanov, A. V. Pluronic-modified superoxide dismutase 1 attenuates angiotensin II-induced increase in intracellular superoxide in neurons. *Free Radical Biol. Med.* **2010**, *49*, 548−558.

(10) Briggs, R. G.; Fee, J. A. Further characterization of human erythrocyte superoxide dismutase. *Biochim. Biophys. Acta, Protein Struct.* **1978**, *537*, 86−99.

(11) Veronese, F. M.; Caliceti, P.; Schiavon, O.; Sergi, M. Polyethylene glycol-superoxide dismutase, a conjugate in search of exploitation. *Adv. Drug Delivery Rev.* **2002**, *54*, 587−606.

(12) Haun, S. E.; Kirsch, J. R.; Helfaer, M. A.; Kubos, K. L.; Traystman, R. J. Polyethylene glycol-conjugated superoxide dismutase fails to augment brain superoxide dismutase activity in piglets. *Stroke* **1991**, *22*, 655−659.

(13) Veronese, F. M.; Caliceti, P.; Pastorino, A.; Schiavon, O.; Sartore, L.; Banci, L.; Scolaro, L. M. Preparation, physico-chemical and pharmacokinetic characterization of monomethoxypoly(ethylene glycol)-derivatized superoxide dismutase. *J. Controlled Release* **1989**, *10*, 145−154.

(14) Yoshida, K.; Burton, G. F.; McKinney, J. S.; Young, H.; Ellis, E. F. Brain and tissue distribution of polyethylene glycol-conjugated superoxide dismutase in rats. *Stroke* **1992**, *23*, 865−869.

(15) Hood, E.; Simone, E.; Wattamwar, P.; Dziubla, T.; Muzykantov, V. Nanocarriers for vascular delivery of antioxidants. *Nanomedicine (London)* **2011**, *6*, 1257−1272.

(16) Han, J.; Shuvaev, V. V.; Muzykantov, V. R. Catalase and superoxide dismutase conjugated with platelet-endothelial cell adhesion molecule antibody distinctly alleviate abnormal endothelial permeability caused by exogenous reactive oxygen species and vascular endothelial growth factor. *J. Pharmacol. Exp. Ther.* **2011**, *338*, 82−91.

(17) Shuvaev, V. V.; Muzykantov, V. R. Targeted modulation of reactive oxygen species in the vascular endothelium. *J. Controlled Release* **2011**, *153*, 56−63.

(18) Shuvaev, V. V.; Tliba, S.; Nakada, M.; Albelda, S. M.; Muzykantov, V. R. Platelet-endothelial cell adhesion molecule-1-directed endothelial targeting of superoxide dismutase alleviates oxidative stress caused by either extracellular or intracellular superoxide. *J. Pharmacol. Exp. Ther.* **2007**, *323*, 450−457.

(19) Choi, Y. J.; Lee, J. Y.; Chung, C. P.; Park, Y. J. Cell-penetrating superoxide dismutase attenuates oxidative stress-induced senescence by regulating the p53-p21(Cip1) pathway and restores osteoblastic differentiation in human dental pulp stem cells. *Int. J. Nanomed.* **2012**, *7*, 5091−5106.

(20) Reukov, V.; Maximov, V.; Vertegel, A. Proteins conjugated to poly(butyl cyanoacrylate) nanoparticles as potential neuroprotective agents. *Biotechnol. Bioeng.* **2011**, *108*, 243−252.

(21) Batrakova, E. V.; Vinogradov, S. V.; Robinson, S. M.; Niehoff, M. L.; Banks, W. A.; Kabanov, A. V. Polypeptide point modifications with fatty acid and amphiphilic block copolymers for enhanced brain delivery. *Bioconjugate Chem.* **2005**, *16*, 793−802.

(22) Yi, X.; Batrakova, E.; Banks, W. A.; Vinogradov, S.; Kabanov, A. V. Protein conjugation with amphiphilic block copolymers for enhanced cellular delivery. *Bioconjugate Chem.* **2008**, *19*, 1071−1077.

(23) Price, T. O.; Farr, S. A.; Yi, X.; Vinogradov, S.; Batrakova, E.; Banks, W. A.; Kabanov, A. V. Transport across the blood-brain barrier of pluronic leptin. *J. Pharmacol. Exp. Ther.* **2010**, *333*, 253−263.

(24) Banks, W. A.; Gertler, A.; Solomon, G.; Niv-Spector, L.; Shpilman, M.; Yi, X.; Batrakova, E.; Vinogradov, S.; Kabanov, A. V. Principles of strategic drug delivery to the brain (SDDB): Development of anorectic and orexigenic analogs of leptin. *Physiol. Behav.* **2011**, *105*, 145−149.

(25) Tong, J.; Luxenhofer, R.; Yi, X.; Jordan, R.; Kabanov, A. V. Protein modification with amphiphilic block copoly(2-oxazoline)s as a new platform for enhanced cellular delivery. *Mol. Pharmaceutics* **2010**, *7*, 984−992.

(26) Luxenhofer, R.; Schulz, A.; Roques, C.; Li, S.; Bronich, T. K.; Batrakova, E. V.; Jordan, R.; Kabanov, A. V. Doubly amphiphilic poly(2-oxazoline)s as high-capacity delivery systems for hydrophobic drugs. *Biomaterials* **2010**, *31*, 4972−4979.

(27) Barz, M.; Luxenhofer, R.; Zentel, R.; Vicent, M. J. Overcoming the PEG-addiction: well-defined alternatives to PEG, from structure-property relationships to better defined therapeutics. *Polym. Chem.* **2011**, *2*, 1900−1918.

(28) Luxenhofer, R.; Han, Y.; Schulz, A.; Tong, J.; He, Z.; Kabanov, A. V.; Jordan, R. Poly(2-oxazoline)s as polymer therapeutics. *Macromol. Rapid Commun.* **2012**, *33* (19), 1613−1631.

(29) Luxenhofer, R.; Sahay, G.; Schulz, A.; Alakhova, D.; Bronich, T. K.; Jordan, R.; Kabanov, A. V. Structure-property relationship in cytotoxicity and cell uptake of poly(2-oxazoline) amphiphiles. *J. Controlled Release* **2011**, *153*, 73−82.

(30) Roe, J. A.; Butler, A.; Scholler, D. M.; Valentine, J. S.; Marky, L.; Breslauer, K. J. Differential scanning calorimetry of Cu,Zn-superoxide dismutase, the apoprotein, and its zinc-substituted derivatives. *Biochemistry* **1988**, *27*, 950−958.

(31) Das, S. K.; Fanburg, B. L. Hyperoxia elevates Cu,Zn-superoxide dismutase of endothelial cells as detected by a sensitive ELISA. *Enzyme* **1992**, *46*, 188−195.

(32) Tsogtbaatar, G.; Tachibana, M.; Watanabe, K.; Kim, S.; Suzuki, H.; Watarai, M. Enzyme-linked immunosorbent assay for screening of canine brucellosis using recombinant Cu-Zn superoxide dismutase. *J. Vet. Med. Sci.* **2008**, *70*, 1387−1389.

(33) Sahay, G.; Alakhova, D. Y.; Kabanov, A. V. Endocytosis of nanomedicines. *J. Controlled Release* **2010**, *145*, 182−195.

(34) Sahay, G.; Batrakova, E. V.; Kabanov, A. V. Different internalization pathways of polymeric micelles and unimers and their effects on vesicular transport. *Bioconjugate Chem.* **2008**, *19*, 2023−2029.

(35) Tong, J.; Zimmerman, M. C.; Li, S.; Yi, X.; Luxenhofer, R.; Jordan, R.; Kabanov, A. V. Neuronal uptake and intracellular superoxide scavenging of a fullerene (C60)-poly(2-oxazoline)s nanoformulation. *Biomaterials* **2011**, *32*, 3654−3665.

(36) Banks, W. A.; Kastin, A. J.; Brennan, J. M.; Vallance, K. L. Adsorptive endocytosis of HIV-1gp120 by blood-brain barrier is enhanced by lipopolysaccharide. *Exp. Neurol.* **1999**, *156*, 165−171.

(37) Blasberg, R. G.; Patlak, C. S.; Fenstermacher, J. D. Selection of experimental conditions for the accurate determination of blood–brain transfer constants from single-time experiments: a theoretical analysis. *J. Cereb. Blood Flow Metab.* **1983**, *3*, 215−225.

(38) Patlak, C. S.; Blasberg, R. G.; Fenstermacher, J. D. Graphical evaluation of blood-to-brain transfer constants from multiple-time uptake data. *J. Cereb. Blood Flow Metab.* **1983**, *3*, 1−7.

(39) Bullock, J.; Chowdhury, S.; Severdia, A.; Sweeney, J.; Johnston, D.; Pachla, L. Comparison of results of various methods used to determine the extent of modification of methoxy polyethylene glycol 5000-modified bovine Cupri-Zinc superoxide dismutase. *Anal. Biochem.* **1997**, *254*, 254−262.

(40) Veronese, F. M.; Sartore, L.; Schiavon, O.; Caliceti, P. A comparative study of enzymatic, structural, and pharmacokinetic properties of superoxide dismutase isolated from two sources and modified by monomethoxypolyethylene glycol using different methods of coupling. *Ann. N.Y. Acad. Sci.* **1990**, *613*, 468−474.

(41) Banci, L.; Bertini, I.; Caliceti, P.; Monsu Scolaro, L.; Schiavon, O.; Veronese, F. M. Spectroscopic characterization of polyethylene-glycol modified superoxide dismutase: 1H NMR studies on its Cu2Co2 derivative. *J. Inorg. Biochem.* **1990**, *39*, 149−159.

(42) Foreman, M. B.; Coffman, J. P.; Murcia, M. J.; Cesana, S.; Jordan, R.; Smith, G. S.; Naumann, C. A. Gelation of amphiphilic lipopolymers at the air-water interface: 2D analogue to 3D gelation of colloidal systems with grafted polymer chains? *Langmuir* **2002**, *19*, 326−332.

(43) Rehfeldt, F.; Tanaka, M.; Pagnoni, L.; Jordan, R. Static and dynamic swelling of grafted poly(2-alkyl-2-oxazoline)s. *Langmuir* **2002**, *18*, 4908−4914.

(44) Shinoda, T.; Takagi, A.; Maeda, A.; Kagatani, S.; Konno, Y.; Hashida, M. In vivo fate of folate-BSA in non-tumor- and tumor-bearing mice. *J. Pharm. Sci.* **1998**, *87*, 1521−1526.

(45) Katsumi, H.; Nishikawa, M.; Yamashita, F.; Hashida, M. Development of polyethylene glycol-conjugated poly-S-nitrosated serum albumin, a novel S-Nitrosothiol for prolonged delivery of nitric oxide in the blood circulation in vivo. *J. Pharmacol. Exp. Ther.* **2005**, *314*, 1117−1124.

(46) Khmelnitsky, Y. L.; Mozhaev, V. V.; Belova, A. B.; Sergeeva, M. V.; Martinek, K. Denaturation capacity: a new quantitative criterion for selection of organic solvents as reaction media in biocatalysis. *Eur. J. Biochem.* **1991**, *198*, 31−41.

(47) Miyamoto, M.; Naka, K.; Shiozaki, M.; Chujo, Y.; Saegusa, T. Preparation and enzymic activity of poly[(N-acylimino)ethylene]-modified catalase. *Macromolecules* **1990**, *23*, 3201−3205.

(48) Viegas, T. X.; Bentley, M. D.; Harris, J. M.; Fang, Z.; Yoon, K.; Dizman, B.; Weimer, R.; Mero, A.; Pasut, G.; Veronese, F. M. Polyoxazoline: chemistry, properties, and applications in drug delivery. *Bioconjugate Chem.* **2011**, *22*, 976−986.

(49) Arakawa, T.; Prestrelski, S. J.; Kenney, W. C.; Carpenter, J. F. Factors affecting short-term and long-term stabilities of proteins. *Adv. Drug Delivery Rev.* **2001**, *46*, 307−326.

(50) Chi, E. Y.; Krishnan, S.; Randolph, T. W.; Carpenter, J. F. Physical stability of proteins in aqueous solution: mechanism and driving forces in nonnative protein aggregation. *Pharm. Res.* **2003**, *20*, 1325−1336.

(51) Mayor, S.; Pagano, R. E. Pathways of clathrin-independent endocytosis. *Nat. Rev. Mol. Cell Biol.* **2007**, *8*, 603−612.

(52) Conner, S. D.; Schmid, S. L. Regulated portals of entry into the cell. *Nature* **2003**, *422*, 37−44.

(53) Richter, C.; Gogvadze, V.; Laffranchi, R.; Schlapbach, R.; Schweizer, M.; Suter, M.; Walter, P.; Yaffee, M. Oxidants in mitochondria: from physiology to diseases. *Biochim. Biophys. Acta* **1995**, *1271*, 67−74.

(54) Dikalov, S.; Griendling, K. K.; Harrison, D. G. Measurement of reactive oxygen species in cardiovascular studies. *Hypertension* **2007**, *49*, 717−727.

(55) Klyachko, N. L.; Manickam, D. S.; Brynskikh, A. M.; Uglanova, S. V.; Li, S.; Higginbotham, S. M.; Bronich, T. K.; Batrakova, E. V.; Kabanov, A. V. Cross-linked antioxidant nanozymes for improved delivery to CNS. *Nanomedicine* **2012**, *8*, 119−129.

(56) Hu, P.; Tirelli, N. Scavenging ROS: superoxide dismutase/catalase mimetics by the use of an oxidation-sensitive nanocarrier/enzyme conjugate. *Bioconjugate Chem.* **2012**, *23*, 438−449.